



Cite this: *Environ. Sci.: Nano*, 2019, 6, 2652

Accelerated Fenton-like kinetics by visible-light-driven catalysis over iron(III) porphyrin functionalized zirconium MOF: effective promotion on the degradation of organic contaminants†

Lei Wang,^{ac} Pengxia Jin,^a Shuhua Duan,^a Jingwei Huang,^{ab} Houde She,^a Qizhao Wang ^{*ac} and Taicheng An ^{*b}

Ultraviolet (UV)-light or a cocatalyst (e.g., chelating agents) is commonly used to promote a Fenton-like technique in the treatment of organic contaminants in wastewater. However, the energy costs for generating UV and the poor recyclability of the iron (Fe)-based catalyst/cocatalyst remain primary concerns for their further implementation. Herein, we present a visible-light-driven collaborative process comprising photocatalysis and Fenton-like reaction that are both conducted using a derivative of a zirconium (Zr)-based metal-organic framework (UiO-66 MOF), in which Fe(III) tetra(4-carboxylphenyl)porphyrin chloride (Fe^{III}-TCPPCl) is coordinated in the pore of UiO-66. The mixed ligand Fe^{III}-TCPPCl not only plays the role of a photosensitizer that fosters light absorption and suppresses the recombination of photo-induced carriers over the integrated structure, Fe^{III}-TCPPCl@UiO-66 (FTU), but also acts as a potential iron-based catalyst for decomposing hydrogen peroxide (H₂O₂) to engender oxidative hydroxyl radicals ([•]OH). Furthermore, besides achieving virtually 100% decomposition of a surrogate pollutant, rhodamine B (RhB), compared with 51% achieved by photolysis alone within 60 min, introducing H₂O₂ into the visible-light irradiating system could also promote the mineralization of RhB, as indicated by a 15.5% increment in chemical oxygen demand (COD) removal. The photo-excited electrons partially participate in the reduction of the immobilized Fe^{III}-TCPPCl into Fe^{II}-TCPPCl and therefore greatly accelerate the Fenton-like reaction. Moreover, the structural similarity of FTU to the robust parent UiO-66 guarantees its reliable recycling performance with respect to degradation over four times.

Received 22nd April 2019,
Accepted 5th July 2019

DOI: 10.1039/c9en00460b

rsc.li/es-nano

Environmental significance

In support of UV light or organic chelating agents, Fenton-like wastewater treatment can achieve the efficient and ameliorated removal of organic contaminants. However, the high production costs of UV systems, and the poor recycling capability of many iron-based catalysts or chelators, still limit its further practical application. Herein, we present a cooperative catalysis consisting of photocatalysis and Fenton-like reaction driven by visible light. The catalyst used is a UiO-66-based MOF that is implanted with a Fe^{III} metalloporphyrin, the coordination modality of which enables the structure to maintain the parental robustness and thus ensure it could be reliably recycled.

^a Research Center of Gansu Military and Civilian Integration Advanced Structural Materials, College of Chemistry and Chemical Engineering, Northwest Normal University, Lanzhou 730070, China. E-mail: wangqizhao@163.com

^b Guangzhou Key Laboratory of Environmental Catalysis and Pollution Control, School of Environmental Science and Engineering, Institute of Environmental Health and Pollution Control, Guangdong University of Technology, Guangzhou, 510006, China. E-mail: antc99@gdut.edu.cn

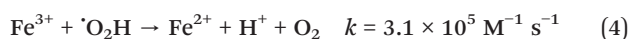
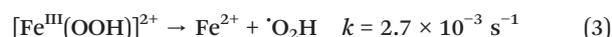
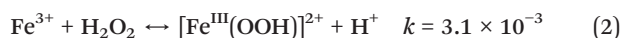
^c Key Laboratory for Photonic and Electronic Bandgap Materials, Ministry of Education, School of Physics and Electronic Engineering, Harbin Normal University, Harbin 150025, China. E-mail: wangqizhao@163.com

† Electronic supplementary information (ESI) available. See DOI: 10.1039/c9en00460b

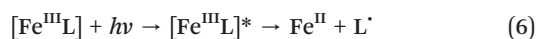
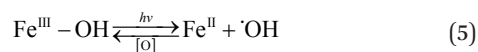
1. Introduction

In recent decades, the advanced oxidation process (AOP) has demonstrated a bright future in wastewater treatment. Relying on the generation of a non-selective oxygen species, hydroxyl radicals ([•]OH) with a standard redox potential of 2.8 V, is capable of decomposing nearly all kinds of organic pollutant.¹ One of the most representative AOP techniques is Fenton process involving ferrous ions (Fe²⁺) that aims at catalyzing the decomposition of hydrogen peroxide (H₂O₂) to produce [•]OH (eqn (1)–(4)).^{2–5} Note that the recovery of Fe²⁺ ions

from homogeneous catalysis is not possible. Iron-based heterogeneous catalysts, *e.g.*, iron oxide,⁶ are used to conduct the so-called Fenton-like process, and consequently allow recycling of the catalyst while reducing the problematic formation of iron sludge that catalytically poisons the reaction and increases the economic burden of the treatment.⁷ In many Fe-based catalysts, iron is primarily present in the form of Fe^{III}, which significantly limits the reaction rate (eqn (2) and (3)).^{2,8}



To address this dilemma, ultraviolet radiation (UV) is generally used to promote the transformation of Fe^{III} into Fe^{II} (eqn (5)).⁹ Nonetheless, this results in other issues; *i.e.*, a harmful influence on human health and increased expenditure. On the other hand, organic chelating ligands, playing the role of ferric chelator (Fe^{III}L) and capable of accelerating the reduction of ferric ions into ferrous ions (eqn (6)),¹⁰ can also be introduced through a Fenton-like technique, such as using ethylenediaminetetraacetic acid (EDTA), nitrilotriacetic acid (NTA), citrate and porphyrin.^{11–14} These so-called cocatalysts, however, might dissolve in treated water and consequently lead to secondary pollution, not to mention their poor recyclability.



Metal–organic frameworks (MOFs),¹⁵ a class of crystalline porous compounds composed of metal clusters that are cross-linked by polyfunctional organic ligands and possessing diverse and tunable structures, have been intensely studied in various practical uses.^{16–20} In their catalytic applications, the high porosity in MOFs could also provide access to sufficient surface active sites for substrate transport.²¹ By selecting robust organic ligands exhibiting oxidative resistance to $\cdot\text{OH}$ and a strong bonding affinity towards iron ions, Fe-based MOFs have been widely investigated in Fenton-like technique.²² For instance, NH₂-MIL-88B(Fe), which is built by the organic linker of 2-aminoterephthalic acid and the metal cluster of Fe^{III}, is able to effectively mineralize methylene blue within a broad working pH range of 3.0–11.0.²³ Moreover, the organic linker plays the role of a photo antenna, and subsequently harvests light and activates metal clusters, favoring linker to metal cluster charge transition, and revealing semiconductor-like behavior of MOFs with the production of oxidative holes (h^+) and reductive electrons

(e^-) (eqn (7)–(10)).^{24,25} Although many MOF structures tend to suffer photo-instability,²⁶ the UiO-66 class, based on Zr₆O₄(OH)₄ secondary building units and dicarboxylate ligands, prefers high crystallinities and thereby exhibits impressive stability under harsh conditions.²⁷ In effect, UiO-66 shows a steady generation of hydrogen in UV-assisted water splitting.²⁸ Moreover, it could act as a photosensitizer for incorporation with some inorganic materials so as to strengthen their light absorption and restrict the recombination of photo-induced carriers, thus ameliorating the photocatalytic performance in degradation against organic pollutants.^{29,30}



Herein, we report a visible-light-driven cooperative process composed of photocatalysis and a simultaneously accelerated Fenton-like reaction that are both catalyzed by a UiO-66 derivative, a structure denoted as Fe^{III}-TCPPCL@UiO-66 (FTU), in which a metalloporphyrin is steadily immobilized through the coordination between the carboxyl (–COOH) in Fe(III) tetra(4-carboxylphenyl)porphyrin chloride (Fe^{III}-TCPPCL) and the zirconium (Zr) cluster in UiO-66.³¹ The mixed ligand Fe^{III}-TCPPCL here not only favors a photosensitization advantage due to its narrow band gap,³² but is also capable of providing a potential iron-based catalyst for decomposing H₂O₂. In fact, the introduction of H₂O₂ can break down rhodamine B (RhB) to virtually 100% within 60 min. The pseudo-first-order rate constant (*k*) of the incorporative process is about 6-times that of photocatalysis alone. Furthermore, it can effectively intensify the mineralization of RhB, as indicated by the chemical oxygen demand (COD) abatement extent rising from 35.0% for photocatalysis alone to 50.5%. In addition, the FTU structure inherits the stability from its parent UiO-66, and thereby presents a steady recycling use of more than four times. The corresponding mechanism for degradation was also conjectured.

2. Experimental

2.1. Materials and synthesis

Details concerning experimental reagents and syntheses are available in ESI† (section S1 for the reagents and S2–S4 for the synthetic procedures).

2.2. Characterizations

The morphology and structure of all composites were observed by JSM-6701E scanning electron microscope (SEM). High-angle annular dark-field scanning transmission electron microscopy (HAADF-STEM) and elemental mapping analysis

were conducted using a JEM-ARM 200F scanning transmission electron microscope. Powder X-ray diffraction (PXRD) measurements were carried out on a Bruker powder X-ray diffraction D8 Advance diffractometer with a monochromatized Cu-K α radiation ($\lambda = 0.15418$ nm) source at 40 kV and 40 mA. Fourier transform infrared (FT-IR) spectroscopy was performed on a Nicolet NEXUS 670 spectrometer. Ultraviolet-visible light diffuse reflectance spectroscopy (UV-vis DRS) was measured using a PuXin TU-1901 UV-vis spectrophotometer equipped with an integrating sphere attachment. The photoluminescence (PL) spectra were measured on a Fluoro Sens 9003 fluorescence spectrophotometer. X-ray photoelectron spectrum (XPS) analysis was recorded on PHI5702 photoelectron spectrometer. The electron spin resonance (ESR) signals of radicals spin-trapped by spin-trapping reagent 5,5-dimethyl-1-pyrroline *N*-oxide (DMPO) were examined *via* a Bruker ER200-SRC spectrometer under visible-light irradiation ($\lambda > 420$ nm) (pH = 3.5). The Brunauer–Emmett–Teller (BET) isotherm was obtained using an Autosorb-iQ2-MP Sorptometer, and the samples were degassed at 120 °C. COD detection was measured using a 5B-3B(H) type COD multi-parameter quick tester of Lian-hua Tech Co., Ltd (detection limit: 0.01 mg L⁻¹). The content of total Fe ions in FTU was measured by USA PE300D inductively coupled plasma optical emission spectrometry (ICP-OES).

2.3. Analytic methods

For the ICP-OES measurement, FTU was digested prior to the detection of the total iron content in the sample. Specifically, a 0.10 g sample (accurate value, 0.0001 g) was loaded into a high-pressure microwave digestion tank. 3.0 mL HNO₃ (~65–68%), 1.0 mL HF ($\geq 40\%$) and 2.0 mL H₂O₂ (30 wt%) were further dropped into the tank in order. The capped tank was shaken and then allowed to stand for 30 min to mix the loaded components evenly. After settling the tank in Ethos 1 Advanced Microwave Digestion (Milestone, Italy), the temperature was gradually increased to 130 °C within 20 min. This condition was maintained for 2 min before continuously warming the digestion system up to 180 °C within 20 min. This state was maintained for 40 min to allow complete digestion of the sample. Subsequently, the mixture in the tank was transferred to a 50 mL clean polytetrafluoroethylene bottle for further ICP determination.

For the ESR measurement, the 'OH and 'O₂⁻ species were trapped by DMPO. 10 mg of the as-prepared samples were dissolved in 0.5 mL of deionized water ('OH) or 0.5 mL of methanol (O₂⁻) and then 45 μ L of DMPO was added followed by ultrasonic dispersion for 5 min.

2.4. Photocurrent measurements

Photocurrent measurements were performed on a CHI-660 electrochemical workstation (Chenhua Instrument, Shanghai, China) in a conventional three-electrode configuration with a Pt foil as the counter electrode and Ag/AgCl (saturated KCl) as the reference electrode. A 300 W Xe arc lamp served as

light source. 0.5 mol L⁻¹ Na₂SO₄ aqueous solution was used as the electrolyte. The working electrodes were prepared as follows: 10.0 mg of the prepared photocatalyst was ground with 10 μ L of a poly (3,4-ethylenedioxythiophene)/poly(styrenesulfonate) (PEDO/TPSS, 1.3–1.7%) aqueous solution and 100 μ L of distilled water to make slurry. The slurry was then spread on a 1.0 \times 1.0 cm fluorine-doped tin oxide (FTO) glass substrate with an active area of about 1.0 cm² by the doctor-blade method, using adhesive tape as the spacer. Finally, the electrode was dried in an oven and annealed at 150 °C for 30 min. Mott–Schottky experiments were conducted on an electrochemical workstation (CHI-660E Instruments) with a standard three-electrode system and an aqueous Na₂SO₄ solution (0.5 mol L⁻¹) as the electrolyte in the dark at 1000 Hz.

2.5. Cooperative catalytic degradation experiments

The cooperative degradation of RhB dominated by UiO-66, TU and FTU was evaluated using an 800 W Xe lamp with a 420 nm UV-cutoff filter under standard conditions (1 atm and 25 \pm 2 °C). The quartz tube with reactant mixtures was set 5 cm away from the light source. 4.0 mg as-prepared sample was added into 40 mL of RhB aqueous solution (30 mg L⁻¹) in a 60 mL cylindrical Pyrex vessel reactor. Before exposure to visible light, the suspension was magnetically stirred in the dark for 0.5 h to reach the adsorption/desorption equilibrium. 10 μ L of the calibrated H₂O₂ (30%, v/v) was then added into the reactor before turning on the lamp. Samples were taken at various intervals (10, 20, 30, 40, 50 and 60 min) to detect RhB content, COD and iron concentration. Centrifugation was operated to separate out the solution for further measurements. With respect to pure photocatalysis, the procedure was similar to the process above, except for the absence of H₂O₂.

3. Results and discussion

3.1. Structure and morphology

The solvothermal reaction of ZrCl₄, terephthalic acid (BDC), Fe^{III}-TCPPCl and benzoic acid (BA) in DMF yielded octahedral microcrystals, FTU, which exhibited an even size distribution due to the SEM in Fig. 1a, demonstrating a similar apparent morphology to that of UiO-66 (Fig. S3a[†]). Due to the inherent fluorescence of Fe^{III}-TCPPCl, the color of FTU was brown (inset of Fig. 1a) as compared with the white color of UiO-66 (inset of Fig. S3a[†]). High-angle annular dark-field scanning transmission electron microscopy (HAADF-STEM) and elemental mapping analysis (Fig. S3b[†]), together with elemental mapping, confirm the existence of the component elements (C, N, O, Fe and Zr) and their homogenous distribution in the entire structure. According to the (111), (002), (022), (004), (115), (224), (046) and (137) crystal facets situated at 7.3°, 8.5°, 12.0°, 17.0°, 22.2°, 25.6°, 30.7° and 33.1°, respectively, as shown in the PXRD patterns (Fig. 1b), the crystalline features of FTU and UiO-66 are consistent.³³

To determine the micro-structure of as-prepared samples, Fourier transform infrared (FT-IR) was initially performed.

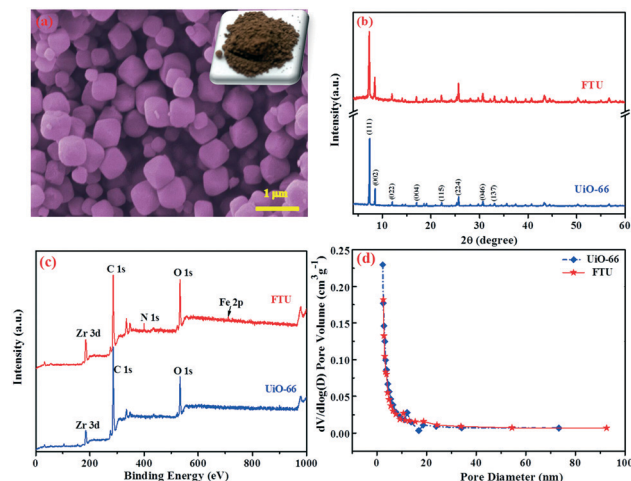


Fig. 1 (a) SEM image of FTU composite (scale bar: 1 μm) (the internal illustration is photograph of FTU); (b) PXRD patterns, (c) XPS survey spectra and (d) Barrett-Joyner-Halenda (BJH) mesoporous size distribution of the UiO-66 and FTU samples.

For both UiO-66 and FTU, signals at 1710, \sim 1626–1630 and 654 cm^{-1} are ascribed to the stretching vibration absorption of C=O, C=C and Zr–O–Zr, respectively (Fig. S4a \dagger).³⁴ The absorption band at 3495 cm^{-1} can be assigned to the stretching vibration absorption of O–H of the adsorbed water in both structures, the hydrophilicity of which guarantee their dispersion in aqueous solution. Significant distinction between these two MOFs lies in the peaks at \sim 1310–1316 cm^{-1} , responsible for C=N as well as the metal ion-centered porphyrin ring in FTU only. In detail, the deformation vibration of the ring increases and a new characteristic absorption peak of Fe–N bond appears at 1000 cm^{-1} ,¹⁴ confirming that Fe^{III}-TCPPCl has been successfully incorporated into UiO-66. The Fe–N bond is also justified by the comparison between FT-IR spectra of TCPP and Fe^{III}-TCPPCl (Fig. S4b \dagger).

To explore the surface chemical composition of the products, wide-scan survey XPS evaluations were carried out. C, O and Zr in UiO-66 were 80.64 wt%, 17.53 wt% and 1.83 wt%, respectively. Owing to the integration of Fe^{III}-TCPPCl, the contents in FTU were changed to 74.48 wt% for C, 22.30 wt% for O, 2.74 wt% for Zr and 0.46 wt% for N (Fig. 1c). Although the measurement for iron was unclear due to its low content, ICP-OES determination revealed that there were 0.3 wt% Fe ions in the integrated structure. The binding energies of C 1s in FTU located at 284.7 eV and 288.5 eV correspond to C–O (N) and –COOH bonds, respectively (Fig. S5a \dagger). The symbolic peaks of the Zr 3d region can be detected as two peaks for Zr 3d_{5/2} and Zr 3d_{3/2} at around 182.7 eV and 185.2 eV, respectively (Fig. S5b \dagger), demonstrating the existence of Zr⁴⁺.^{35,36} The featured signals of O 1s and N 1s are located at 531.7 and 399.7 eV, respectively (Fig. S5c and d \dagger).^{37,38}

To investigate the incorporation mode of Fe^{III}-TCPPCl in FTU, series control trials were operated according to a previous investigation on a similar structure, Ni^{II}-TCPPCl/UiO-66, in which Ni^{II}-TCPPCl was coordinated as a mixed ligand

in UiO-66.³¹ Specifically, a comparison between the ¹H-NMR spectra of digested compounds derived from the post-modified UiO-66 (PMU) by Fe^{III}-TCPPCl and FTU was first conducted (detailed preparation and ¹H-NMR detection procedures are given in section S9 and 10). UiO-66 was synthesized under the same conditions as FTU in the absence of Fe^{III}-TCPPCl, and afterwards was directly mixed with Fe^{III}-TCPPCl to achieve PMU. The obtained PMU was thoroughly washed with pure water to remove the remaining Fe^{III}-TCPPCl, giving a light brown product (Fig. S6a \dagger) for the ensuing ¹H-NMR detection (Fig. S7 \dagger). Unfortunately, the digested compounds only present a strong characteristic signal of BDC at δ 8.00 ppm without characteristic peaks of Fe^{III}-TCPPCl at δ 8.32 or 8.80 ppm, suggesting that the light brown color is primarily driven by the weak attachment of Fe^{III}-TCPPCl on the outer surface of UiO-66 (Fig. S6b(i) \dagger). In contrast, the compound resulting from the digestion of the washed FTU (Fig. S6b(ii) \dagger) evidently presents featured signals of both BDC and Fe^{III}-TCPPCl (Fig. S8 \dagger). Moreover, the total pore volume of the MOF structure decreases from 0.565 $\text{cm}^3 \text{g}^{-1}$ to 0.471 $\text{cm}^3 \text{g}^{-1}$ after the incorporation of Fe^{III}-TCPPCl and UiO-66 (Fig. 1d). Due to the previous study on Ni^{II}-TCPPCl/UiO-66, it is considered that the majority of the pores in FTU are randomly occupied by Fe^{III}-TCPPCl. To further confirm this consideration, Fe^{III}-TCPPCl was replaced by Fe(III) tetra(4-phenyl)porphyrin chloride (Fe^{III}-TPPCL) in an analogous size to conduct the same preparation procedure. Without the coordinative substituent –COOH, the achieved product can be easily washed to a white color (Fig. S6b(iii) \dagger), and the ¹H-NMR spectrum of the accordingly digested compound exhibits an undetectable characteristic signal for Fe^{III}-TPPCL. Therefore, a large proportion of the Fe^{III}-TCPPCl molecules are integrated in the pores through coordination between –COOH in Fe^{III}-TCPPCl and Zr cluster in UiO-66, other than simply being attached on the outer surface of UiO-66 or merely encapsulated in the pores of UiO-66.³⁹ Immobilization of metalloporphyrin derivatives into MOFs through coordination to form an integral structure is valuable since the strong binding can keep them from aggregation and formation of catalytically inactive dimers, thereby prolonging their lifetime for catalytic use.⁴⁰

3.2. Optical feature and photoelectrochemical measurement

The optical properties of the MOF samples were measured using UV-vis DRS (Fig. S9a and b \dagger). The implantation of metal porphyrin into zirconium-based MOF significantly enables the absorption edge to shift towards the long-wave direction in comparison with UiO-66 (Fig. S9b \dagger). According to $\alpha h\nu = A(h\nu - E_g)^2$ where α , ν , A and E_g are absorption coefficient, light frequency, proportionality constant and indirect band gap energy, respectively. The indirect bandgap of UiO-66 was calculated as 3.66 eV (Fig. S9c \dagger), while the calculation gives the value of Fe^{III}-TCPPCl as 1.65 eV (Fig. S9d \dagger). In fact, the light absorption edge can be extended to around 700 nm by the integrated Fe^{III}-TCPPCl. As revealed by the

photoluminescence (PL) spectra of UiO-66 and FTU (Fig. S9e†), a strong peak at 468 nm is observed for UiO-66, while a weak signal at the same location can be found for FTU. This significant decrement in fluorescence peak intensity indicates that the recombination rate of photo-induced electrons and holes in the FTU composite is attenuated. To ascertain the suppression, Mott–Schottky measurements on both photoanodes were conducted at frequencies of 1000 Hz. The positive slope of the obtained C^{-2} to the potential plot is consistent with that of typical n-type semiconductors, and the derived flat-band potential for UiO-66 is -0.60 V *vs.* Ag/AgCl (Fig. S10†). Considering the small difference between the flat-band potential and the lower CB edge for n-type semiconductors, the conduction band minimum (CBM) position of UiO-66 can be roughly estimated to be -0.62 V (*vs.* reversible hydrogen electrode [RHE]) (Fig. S10a†). With the bandgap energy of UiO-66 estimated as 3.66 eV according to the Tauc plot (Fig. S9c†), its valence band maximum (VBM) position was then calculated to be $+3.04$ V (*vs.* RHE). Associating with the corresponding band gaps, the energy level of the lowest unoccupied molecular orbital (LUMO) and highest occupied molecular orbital (HOMO) of Fe^{III} -TCPPCl were roughly estimated as -0.68 V (Fig. S10b†) and 0.97 V, respectively, while the VBM and the CBM of UiO-66 that favors n-type semiconductor feature⁴¹ are approximately 3.04 V and -0.62 V, respectively. Due to the standard redox potential of Fe^{3+} ($E_{\text{Fe}^{3+}/\text{Fe}^{2+}}^0 = 0.771$ V), it is probable that the core center (Fe^{III}) of Fe^{III} -TCPPCl plays the role of trap site for the photo-induced electrons, and consequently reduces the charge recombination to some extent.^{42,43} In fact, the photoelectrochemical measurements indicate that the transient photocurrent density increases from 0.0025 mA cm^{-2} of UiO-66 to 0.0056 mA cm^{-2} of FTU (Fig. S9f†).

3.3. Cooperative catalytic performance

In order to closely investigate the collaborative catalysis, series catalytic operations were implemented under different situations. In the dark, both of the MOFs, UiO-66 and FTU, display virtually the same slight RhB removals, which might be due to their analogous skeleton structures possessing similar adsorption abilities toward RhB ($<7\%$, Fig. S11†). In a proof-of-concept that FTU is capable of playing dual-catalytic performance in assistance of visible-light ($\lambda > 420$ nm) (*i.e.*, photocatalysis and Fenton-like reaction), photocatalytic reactions over the as-prepared samples were first conducted in the absence of H_2O_2 . FTU/*vis* photocatalysis can decompose 51% RhB within 60 min, which is 25% and 27% higher than that of UiO-66/*vis* and that of the Fe^{III} -TCPPCl/*vis* reaction, respectively (Fig. 2a). The significant improvement by contrast to UiO-66 can be explained by the optical advantages justified by DRS and PL detection (Fig. S9†).

In the presence of H_2O_2 , there should coexist a Fenton-like reaction creating a nonnegligible effect on the degradation of RhB due to the reduction of Fe^{III} -TCPPCl into Fe^{II} -TCPPCl under light irradiation that promotes the reaction ki-

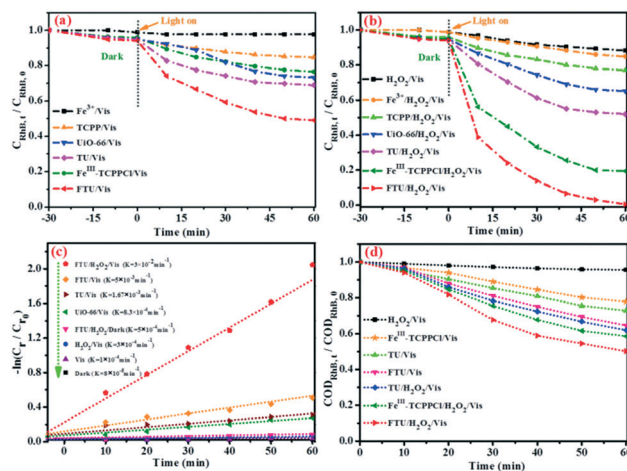
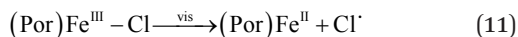


Fig. 2 (a) Degradation of RhB by different catalysts in visible-light system; (b) degradation of RhB by different catalysts in visible light and H_2O_2 system; (c) pseudo-first-order kinetics curves and apparent reaction rate constants k -value of the degradation of RhB under different conditions; (d) COD testing of RhB mineralization under different conditions. Original dosage of the reactants and catalyst: $[\text{C}_{\text{RhB}}]_0 = 30$ mg L^{-1} , $[\text{Fe}^{3+}]_0 = 0.3$ mg L^{-1} , $[\text{TCPP}, \text{Fe}^{\text{III}}\text{-TCPPCl}, \text{UiO-66}, \text{TU}$ and $\text{FTU}]_0 = 0.10$ g L^{-1} , $[\text{H}_2\text{O}_2]_0 = 2.5$ mM, pH = 3.5 and temperature = 25 ± 2 °C.

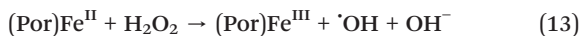
netics (eqn (11)).⁴⁴ When both FTU and H_2O_2 were present in the visible-light irradiating system (Fig. 2b), the degrading extent is 37% greater than the theoretical sum (63%) of degradation by H_2O_2 and decomposition *via* FTU/*vis*. According to pseudo-first-order model (eqn (12)), where C denotes the RhB concentration at the time interval t , and C_0 represents the initial RhB concentration, the reaction rate constant k is about 6-times that of FTU/*vis* operation alone (Fig. 2c). In addition, the mineralization degree of the dye is also greatly enhanced, as revealed by the COD removal extent increasing from 35% by FTU/*vis* to 50.5% of the cooperative process (Fig. 2d).

To provide a concrete justification for the coexistent Fenton-like reaction, a list of control degradation trials was designed. As presented in Fig. 2b, owing to the virtually equal RhB decomposition degree in TU/ H_2O_2 /*vis* treatment (48%) to a theoretical total value of RhB removal by H_2O_2 /*vis* (12%) and TU/*vis* (32%), it is considered that the TU component rarely participates in the H_2O_2 involved reaction. Thus, the interaction between the coordinated Fe^{3+} iron or the integrated Fe^{III} -TCPPCl and coexistent H_2O_2 should be taken into account for the demonstration of the nearly complete RhB decrement *vs.* 51% RhB removal in FTU/*vis* system. As revealed in Fig. 2b, the visible light irradiating Fe^{3+} / H_2O_2 system provides only 15% removal of RhB due to its inferior kinetics in the absence of UV light.¹ In contrast, when the ferric ion was replaced by the slightly soluble Fe^{III} -TCPPCl,⁴⁵ the degradation extent of Fe^{III} -TCPPCl/ H_2O_2 increases to 80%, along with 41% diminished COD (Fig. 2d). In contrast, TCPP/ H_2O_2 achieves only 23% decomposition of the dye. The lower removal degree of Fe^{III} -TCPPCl/ H_2O_2 /*vis* than that of FTU/ H_2O_2 /*vis* can be attributed to the abundant active sites and accelerated charge transfer capacitated by the MOF

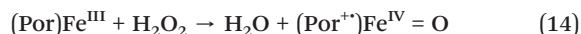
structure. Consequently, the consideration that H_2O_2 decomposition is catalyzed by Fe^{III} -TCPPCl in the presence of visible light, with additional generation of $\cdot\text{OH}$ accounting for the enhanced degradation of RhB is definitely ascertained (eqn (13), Por = porphyrin ligand).^{14,44}



$$-\ln(C/C_0) = kt \quad (12)$$



Under neutral or alkaline conditions, another interaction between H_2O_2 and Fe^{III} -TCPPCl might also take place. Specifically, it is the activation of hydrogen peroxide by direct contact between the coordinated Fe^{III} center in porphyrin and H_2O_2 , resulting in a transient high-valent oxo-iron species with oxidative capability, $(\text{Por}^+)\text{Fe}^{\text{IV}}=\text{O}$ ($E^0 = 1.80$ V, pH at 7, eqn (14) and (15)).^{46,47} However, since Fenton kinetics is crucially relevant to pH value and other factors, we fixed the optimal reaction situation match: pH value of 3.5, 0.10 g L^{-1} and 2.5 mM for the initial concentration of $[\text{FTU}]_0$ and $[\text{H}_2\text{O}_2]_0$, respectively (Fig. S12–S14†). Given the acidic ambience for the catalytic operation, the influence of $(\text{Por}^+)\text{Fe}^{\text{IV}}=\text{O}$ on the final degradation can be excluded.



In addition, we selected several iron complexes based heterocatalysts to make a degradation efficiency comparison with FTU (Table S1†). As compared with the Fe-based MOFs, FTU can degrade the pollutant surrogate with less Fenton agent; in comparison with the Fe complex-immobilized heterocatalysts that employ UV light, FTU is able to achieve an effective degradation with the assistance of visible light.

3.4. Stability and recyclability

To verify the stability of FTU during its catalytic use, the total dissolved iron in the treated water over time was collected by ICP. The leached irons account for 0.06% of the total irons in the reaction solution, indicating that few integrated Fe^{III} -TCPPCl molecules leach out from FTU during the degradation process (Fig. S15a†). Meanwhile, each centrifuged solution sample without FTU was further irradiated by visible light to identify whether there was further decomposition of RhB. However, undetectably continuous abatement in RhB concentration is observed (Fig. S15b†). Hence, the catalyst maintains its structure well during the catalysis, and the entire degradation is a heterogeneous reaction rather than a homogeneous process, meaning that either pollutant surrogate or H_2O_2 should be adsorbed to the surface of FTU prior to its continuous reaction.⁴⁸

In order to further confirm its recycling performance, FTU was employed for a 4-time degradation test (Fig. 3a). More than 94% RhB removal was achieved for each run, indicating an excellent reusability of the photocatalyst. Moreover, the recycled catalyst still sustains well after the four-time employment, as revealed by the SEM (Fig. 3b), PXRD and FT-IR detection (Fig. 3c and d), all of which suggest a high morphology and composition similarity to the original FTU. This unique robustness can be attributed to the virtual structural identity between FTU and its parent MOF, UiO-66, which is considered to be one of the most stable MOFs capable of bearing harsh chemical conditions while sustaining its crystallinity.^{27,49} Furthermore, the steady coordination mode of the incorporated Fe^{III} -TCPPCl in the MOF pores prohibits its leaking.³¹

3.5. Identification of the primary reactive oxidants

Commonly, three reactive oxidants, photo-induced holes (h^+), $\cdot\text{OH}$ and $\cdot\text{O}_2^-$, are commonly regarded as possible radical species in photocatalysis, while the latter two are also involved in Fenton-like reactions. To verify their impacts on the degradation, *tert*-butanol (TBA), ammonium oxalate (AO) and *p*-benzoquinone (BQ) were used as the scavengers for $\cdot\text{OH}$, h^+ and $\cdot\text{O}_2^-$, respectively (Fig. S16†).⁵⁰ FTU/vis system gives 51% degradation of the contaminant, but as TBA and AO were added, significant loss in removal extents were found (Fig. S16a†). In contrast, the introduction of BQ leads to relatively slight decline in degradation degree. Hence, $\cdot\text{OH}$, h^+ and $\cdot\text{O}_2^-$ are involved in the photocatalytic degradation, and the former two are crucial. The generation of the latter two oxidants is due to the fact that the VBM and CBM positions of UiO-66 are located at $+3.04$ V (*vs.* RHE) and -0.62 V (*vs.* RHE), respectively. Therefore, both the oxidation of adsorbed OH^- and H_2O to $\cdot\text{OH}$ ($+1.9$ eV *vs.* NHE, pH = 4 ($E_{\text{H}_2\text{O}/\cdot\text{OH}} = 2.73$ V)) as

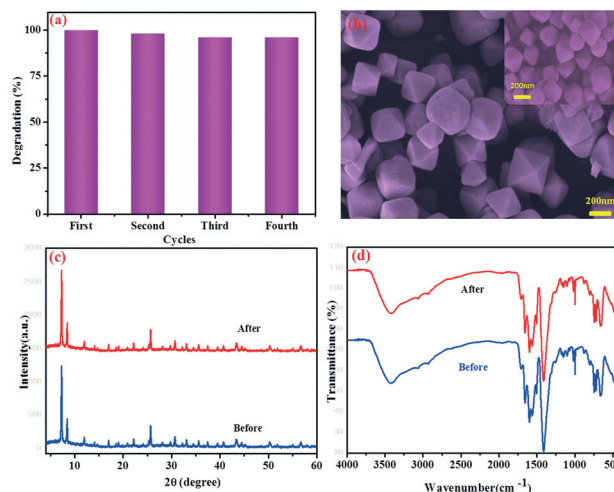
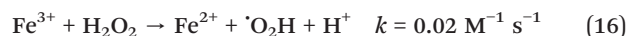


Fig. 3 (a) Degradation of RhB over FTU composite at multiple regeneration cycles; (b) SEM spectra of FTU after catalytic reaction; (c) XRD patterns and (d) FT-IR spectra of FTU before and after catalytic reaction.

well as the reduction of adsorbed O_2 into $\cdot O_2^-$ (-0.33 V vs. NHE) can be thermodynamically actualized⁵¹ by the photo-excited carriers. The ESR detections justify the presence of an $\cdot OH$ radical that features quartet peaks and four corresponding troughs of DMPO- $\cdot OH$ adduct with a 1:2:2:1 ratio (Fig. 4a and b), as well as $\cdot O_2^-$ matters that characterizes sextet peaks of DMPO- $\cdot O_2^-$ (Fig. 4c and d).^{52,53} As compared with no characteristic signal in the dark, both of their intensities increased over time when the light was turned on.

For the FTU/ H_2O_2 /vis system, the addition of TBA, AO and BQ reduce the degradation extents to 87.3%, 41.9% and 50%, respectively (Fig. S16b†). The effects caused by all three active species are amplified in comparison with those of FTU/vis. The greater impact of h^+ can be attributed to the advanced suppression against the recombination of photo-induced charges. As mentioned above in the photocatalytic measurements, the unoccupied Fe^{III} traps levels between the VBM and the CBM of UiO-66 not only traps the electrons that generated by the light excited metalloporphyrin, Fe^{III} -TCPPCl*, but also captures the electrons that transferred to the VBM of UiO-66 to implement the reduction of the core metal Fe^{3+} into Fe^{2+} .¹⁴ In the presence of H_2O_2 , the Fenton-like reaction further promotes the trapping process, and thus restricts the recombination with a higher h^+ generation. On the other hand, the transformation of Fe^{3+} to Fe^{2+} in turn greatly accelerates the Fenton-like reaction, and consequently gives a greater production of $\cdot OH$ that propels the decomposition extent. Thus, $\cdot OH$ is still the primary radical responsible for the removal of RhB. In FTU/ H_2O_2 /vis catalysis, however, the contribution of h^+ to the degradation becomes less than that of $\cdot O_2^-$, which is opposite to the result in the FTU/vis operation. It can be also ascribed to the addition of H_2O_2 , which brings up chain reaction of the Fenton-like process and therefore produces more $\cdot O_2H$ matters (eqn (16)).⁵⁴ Moreover, the ESR detection further ascertains the increased reactive oxygen species (ROS). As shown in Fig. 4, the signal intensities of

both $\cdot OH$ and $\cdot O_2^-$ (eqn (17)) in FTU/ H_2O_2 /vis (Fig. 4b and d) are augmented relative to those of FTU/vis (Fig. 4a and c).



3.6. Mechanism investigation

The primary mechanism was proposed, as seen in Fig. 5. When FTU was irradiated by visible light, the integrated Fe^{III} -TCPPCl turned into an excited state and ejected electrons to the CBM of UiO-66, where the adsorbed O_2 was reduced by the electrons to form $\cdot O_2^-$, a critical radical during the ring cleavage of aromatic intermediate compounds.⁵⁵ The generated h^+ in VBM and the accordingly generated $\cdot OH$ through the oxidation of adsorbed H_2O or OH^- by h^+ would further intensify the decomposition of the pollutant. Note that the Fe^{III} core of Fe^{III} -TCPPCl performs the role of trapping site for the electrons; therefore, in addition to the confinement of the recombination of photo-induced carriers, the obtained Fe^{II} -TCPPCl would catalyze the decomposition of added H_2O_2 in a rapid reaction kinetic with greater $\cdot OH$ and $\cdot O_2^-$ production (eqn (1)-(4)).⁵⁶ In particular, the hydroxyl radicals are capable of intensifying the mineralization of RhB into CO_2 and H_2O .

4. Conclusions

In summary, a UiO-66 derivative, in which Fe^{III} -TCPPCl is integrated by a coordination mode, was used for the catalytic application of the degradation of RhB. Through the reduction of the Fe^{3+} core into Fe^{2+} by the photo-generated electrons, the obtained FTU structure is able to catalyze the Fenton-like reaction with an accelerated reaction rate and enhanced generation of $\cdot OH$ radicals in the presence of H_2O_2 . The reduction performance also improves the separation of photo-induced charges, and thus produced more h^+ . According to the scavenging trials and ESR measurements, h^+ and $\cdot OH$ are the major oxidants that account for the deep breakdown of the contaminant in the cooperative catalytic process comprising photocatalysis and the Fenton-like reaction. This study provides a new method to exploit organic ligands for the purpose of steadily promoting a Fenton-like reaction under

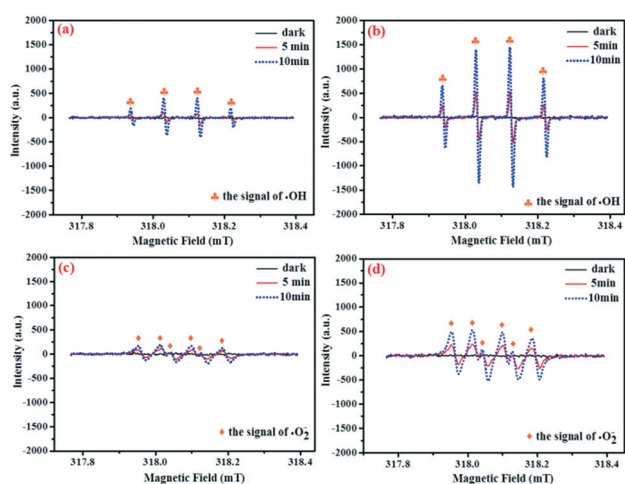


Fig. 4 ESR spectra of radical adducts trapped by (a and b) DMPO- $\cdot OH$ and (c and d) DMPO- $\cdot O_2^-$ either in the dark or under visible-light irradiation of FTU/vis system and FTU/ H_2O_2 /vis system.

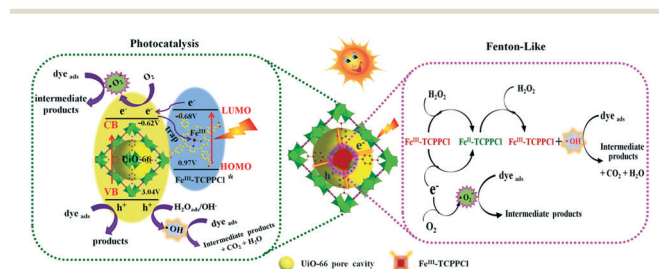


Fig. 5 The proposed photocatalytic mechanism of Fe^{III} -TCPPCl@UiO-66 co-catalytic Fenton-like reaction.

visible-light irradiation with significant removal of organic pollutants in wastewater.

Conflicts of interest

The authors declare no conflict financial interest.

Acknowledgements

This work was financially supported by the National Natural Science Foundation of China (21663027, 21808189), the Fundamental Research Funds for the Central Universities of Chang'an University (300102299304), the Science and Technology Support Project of Gansu Province (1504GKCA027), the Opening Project of Guangzhou Key Laboratory of Environmental Catalysis and Pollution Control (GKLEPC-12).

Notes and references

- S. Rahim Pouran, A. R. Abdul Aziz and W. M. A. Wan Daud, Review on the main advances in photo-Fenton oxidation system for recalcitrant wastewaters, *J. Ind. Eng. Chem.*, 2015, **21**, 53–69.
- D. B. Miklos, C. Remy, M. Jekel, K. G. Linden, J. E. Drewes and U. Hubner, Evaluation of advanced oxidation processes for water and wastewater treatment—A critical review, *Water Res.*, 2018, **139**, 118–131.
- M. Xing, W. Xu, C. Dong, Y. Bai, J. Zeng, Y. Zhou, J. Zhang and Y. Yin, Metal sulfides as excellent co-catalysts for H₂O₂ decomposition in advanced oxidation processes, *Chem*, 2018, **4**, 1359–1372.
- C. Dong, J. Ji, B. Shen, M. Xing and J. Zhang, Enhancement of H₂O₂ decomposition by the co-catalytic effect of WS₂ on the Fenton reaction for the synchronous reduction of Cr(VI) and remediation of phenol, *Environ. Sci. Technol.*, 2018, **52**, 11297–11308.
- J. Liu, C. Dong, Y. Deng, J. Ji, S. Bao, C. Chen, B. Shen, J. Zhang and M. Xing, Molybdenum sulfide co-catalytic Fenton reaction for rapid and efficient inactivation of *Escherichia coli*, *Water Res.*, 2018, **145**, 312–320.
- M. Usman, J. M. Byrne, A. Chaudhary, S. Orsetti, K. Hanna, C. Ruby, A. Kappler and S. B. Haderlein, Magnetite and green rust: synthesis, properties, and environmental applications of mixed-valent iron minerals, *Chem. Rev.*, 2018, **118**, 3251–3304.
- Y. Deng and J. D. Englehardt, Treatment of landfill leachate by the Fenton process, *Water Res.*, 2006, **40**, 3683–3694.
- W. P. Kwan and B. M. Voelker, Rates of hydroxyl radical generation and organic compound oxidation in mineral-catalyzed Fenton-like systems, *Environ. Sci. Technol.*, 2003, **37**, 1150–1158.
- X. Liu, Y. Zhou, J. Zhang, L. Luo, Y. Yang, H. Huang, H. Peng, L. Tang and Y. Mu, Insight into electro-Fenton and photo-Fenton for the degradation of antibiotics: mechanism study and research gaps, *Chem. Eng. J.*, 2018, **347**, 379–397.
- R. G. Zepp, B. C. Faust and J. Hoigne, Hydroxyl radical formation in aqueous reactions (pH 3–8) of iron(II) with hydrogen peroxide: the photo-Fenton reaction, *Environ. Sci. Technol.*, 1992, **26**, 313–319.
- K. Xiao, K. Pei, H. Wang, W. Yu, S. Liang, J. Hu, H. Hou, B. Liu and J. Yang, Citric acid assisted Fenton-like process for enhanced dewaterability of waste activated sludge with in-situ generation of hydrogen peroxide, *Water Res.*, 2018, **140**, 232–242.
- Y. Zhang, P. Chelme-Ayala, N. Klammerth and M. Gamal El-Din, Application of UV-irradiated Fe(III)-nitrilotriacetic acid (UV-Fe(III)NTA) and UV-NTA-Fenton systems to degrade model and natural occurring naphthenic acids, *Chemosphere*, 2017, **179**, 359–366.
- Amina, X. Si, K. Wu, Y. Si and B. Yousaf, Synergistic effects and mechanisms of hydroxyl radical-mediated oxidative degradation of sulfamethoxazole by Fe(II)-EDTA catalyzed calcium peroxide: implications for remediation of antibiotic-contaminated water, *Chem. Eng. J.*, 2018, **353**, 80–91.
- L. Shi, L. Yang, H. Zhang, K. Chang, G. Zhao, T. Kako and J. Ye, Implantation of iron(III) in porphyrinic metal organic frameworks for highly improved photocatalytic performance, *Appl. Catal., B*, 2018, **224**, 60–68.
- J. D. Xiao and H. L. Jiang, Metal-organic frameworks for photocatalysis and photothermal catalysis, *Acc. Chem. Res.*, 2018, **52**, 356–366.
- I. Stassen, N. Burtch, A. Talin, P. Falcaro, M. Allendorf and R. Ameloot, An updated roadmap for the integration of metal-organic frameworks with electronic devices and chemical sensors, *Chem. Soc. Rev.*, 2017, **46**, 3185–3241.
- Z. Zhao, X. Ma, A. Kasik, Z. Li and Y. S. Lin, Gas separation properties of metal organic framework (MOF-5) membranes, *Ind. Eng. Chem. Res.*, 2012, **52**, 1102–1108.
- M. Alvaro, E. Carbonell, B. Ferrer, F. X. Llabres i Xamena and H. Garcia, Semiconductor behavior of a metal-organic framework (MOF), *Chem. – Eur. J.*, 2007, **13**, 5106–5112.
- T. R. Cook, Y. R. Zheng and P. J. Stang, Metal-organic frameworks and self-assembled supramolecular coordination complexes: comparing and contrasting the design, synthesis, and functionality of metal-organic materials, *Chem. Rev.*, 2013, **113**, 734–777.
- D. Farrusseng, S. Aguado and C. Pinel, Metal-organic frameworks: opportunities for catalysis, *Angew. Chem., Int. Ed.*, 2009, **48**, 7502–7513.
- T. Zeng, X. Zhang, S. Wang, H. Niu and Y. Cai, Spatial confinement of a Co₃O₄ catalyst in hollow metal-organic frameworks as a nanoreactor for improved degradation of organic pollutants, *Environ. Sci. Technol.*, 2015, **49**, 2350–2357.
- M. Cheng, C. Lai, Y. Liu, G. Zeng, D. Huang, C. Zhang, L. Qin, L. Hu, C. Zhou and W. Xiong, Metal-organic frameworks for highly efficient heterogeneous Fenton-like catalysis, *Coord. Chem. Rev.*, 2018, **368**, 80–92.
- J. He, Y. Zhang, X. Zhang and Y. Huang, Highly efficient Fenton and enzyme-mimetic activities of NH₂-MIL-88B(Fe) metal organic framework for methylene blue degradation, *Sci. Rep.*, 2018, **8**, 5159.

- 24 S. Wang and X. Wang, Multifunctional metal–organic frameworks for photocatalysis, *Small*, 2015, **11**, 3097–3112.
- 25 Y. Duan, J. Luo, S. Zhou, X. Mao, M. W. Shah, F. Wang, Z. Chen and C. Wang, TiO₂-supported Ag nanoclusters with enhanced visible light activity for the photocatalytic removal of NO, *Appl. Catal., B*, 2018, **234**, 206–212.
- 26 J. J. Low, A. I. Benin, J. Paulina, J. F. Abrahamian, S. A. Faheem and R. R. Willis, Virtual high throughput screening confirmed experimentally: porous coordination polymer hydration, *J. Am. Chem. Soc.*, 2009, **131**, 15834–15842.
- 27 J. B. DeCoste, G. W. Peterson, H. Jasuja, T. G. Glover, Y. G. Huang and K. S. Walton, Stability and degradation mechanisms of metal–organic frameworks containing the Zr₆O₄(OH)₄ secondary building unit, *J. Mater. Chem. A*, 2013, **1**, 5642–5650.
- 28 J. J. Zhou, R. Wang, X. L. Liu, F. M. Peng, C. H. Li, F. Teng and Y. P. Yuan, In situ growth of CdS nanoparticles on UiO-66 metal–organic framework octahedrons for enhanced photocatalytic hydrogen production under visible light irradiation, *Appl. Surf. Sci.*, 2015, **346**, 278–283.
- 29 J. Ding, Z. Yang, C. He, X. Tong, Y. Li, X. Niu and H. Zhang, UiO-66(Zr) coupled with Bi₂MoO₆ as photocatalyst for visible–light promoted dye degradation, *J. Colloid Interface Sci.*, 2017, **497**, 126–133.
- 30 Z. Sha, H. S. Chan and J. Wu, Ag₂CO₃/UiO-66(Zr) composite with enhanced visible–light promoted photocatalytic activity for dye degradation, *J. Hazard. Mater.*, 2015, **299**, 132–140.
- 31 Y. Sun, L. Sun, D. Feng and H. C. Zhou, An in situ one–pot synthetic approach towards multivariate zirconium MOFs, *Angew. Chem.*, 2016, **128**, 6581–6585.
- 32 L. Wang, S. Duan, P. Jin, H. She, J. Huang, Z. Lei, T. Zhang and Q. Wang, Anchored Cu(II) tetra(4–carboxylphenyl)porphyrin to P25 (TiO₂) for efficient photocatalytic ability in CO₂ reduction, *Appl. Catal., B*, 2018, **239**, 599–608.
- 33 X. Tian, Z. Jiang, Y. Fan, S. Qiu, L. Zhang, X. Li, Z. Zhou, T. Liu, Q. Ma, X. Lu, B. Zhong and R. Zhou, A tetravalent vaccine comprising hexon-chimeric adenoviruses elicits balanced protective immunity against human adenovirus types 3, 7, 14 and 55, *Antiviral Res.*, 2018, **154**, 17–25.
- 34 N. Sadeghi, S. Sharifnia and M. Sheikh Arabi, A porphyrin-based metal organic framework for high rate photoreduction of CO₂ to CH₄ in gas phase, *J. CO₂ Util.*, 2016, **16**, 450–457.
- 35 L. Chen, B. Huang, X. Qiu, X. Wang, R. Luque and Y. Li, Seed-mediated growth of MOF-encapsulated Pd@Ag core-shell nanoparticles: toward advanced room temperature nanocatalysts, *Chem. Sci.*, 2016, **7**, 228–233.
- 36 L. Wang, P. Jin, S. Duan, H. She, J. Huang and Q. Wang, In-situ incorporation of Copper(II) porphyrin functionalized zirconium MOF and TiO₂ for efficient photocatalytic CO₂ reduction, *Sci. Bull.*, 2019, **64**, 926–933.
- 37 Y. Liu, Y. Yang, Q. Sun, Z. Wang, B. Huang, Y. Dai, X. Qin and X. Zhang, Chemical adsorption enhanced CO₂ capture and photoreduction over a copper porphyrin based metal organic framework, *ACS Appl. Mater. Interfaces*, 2013, **5**, 7654–7658.
- 38 P. M. Usov, B. Huffman, C. C. Epley, M. C. Kessinger, J. Zhu, W. A. Maza and A. J. Morris, Study of electrocatalytic properties of metal–organic framework PCN-223 for the oxygen reduction reaction, *ACS Appl. Mater. Interfaces*, 2017, **9**, 33539–33543.
- 39 P. Deria, W. Bury, I. Hod, C. W. Kung, O. Karagiari, J. T. Hupp and O. K. Farha, MOF functionalization via solvent-assisted ligand incorporation: phosphonates vs carboxylates, *Inorg. Chem.*, 2015, **54**, 2185–2192.
- 40 C. Y. Lee, O. K. Farha, B. J. Hong, A. A. Sarjeant, S. T. Nguyen and J. T. Hupp, Light-harvesting metal–organic frameworks (MOFs): efficient strut-to-strut energy transfer in bodipy and porphyrin-based MOFs, *J. Am. Chem. Soc.*, 2011, **133**, 15858–15861.
- 41 Y. P. Yuan, L. S. Yin, S. W. Cao, G. S. Xu, C. H. Li and C. Xue, Improving photocatalytic hydrogen production of metal–organic framework UiO-66 octahedrons by dye-sensitization, *Appl. Catal., B*, 2015, **168–169**, 572–576.
- 42 X. Meng, Q. Yu, G. Liu, L. Shi, G. Zhao, H. Liu, P. Li, K. Chang, T. Kako and J. Ye, Efficient photocatalytic CO₂ reduction in all-inorganic aqueous environment: cooperation between reaction medium and Cd(II) modified colloidal ZnS, *Nano Energy*, 2017, **34**, 524–532.
- 43 L. Huang, J. Yang, X. Wang, J. Han, H. Han and C. Li, Effects of surface modification on photocatalytic activity of CdS nanocrystals studied by photoluminescence spectroscopy, *Phys. Chem. Chem. Phys.*, 2013, **15**, 553–560.
- 44 J. Bonin, M. Chaussemier, M. Robert and M. Routier, Homogeneous photocatalytic reduction of CO₂ to CO using iron(0) porphyrin catalysts: mechanism and intrinsic limitations, *ChemCatChem*, 2014, **6**, 3200–3207.
- 45 M. Hoshino, K. Ozawa, H. Seki and P. C. Ford, Photochemistry of nitric oxide adducts of water-soluble iron(III) porphyrin and ferrihemoproteins studied by nano-second laser photolysis, *J. Am. Chem. Soc.*, 1993, **115**, 9568–9575.
- 46 J. He, X. Yang, B. Men and D. Wang, Interfacial mechanisms of heterogeneous Fenton reactions catalyzed by iron-based materials: A review, *J. Environ. Sci.*, 2016, **39**, 97–109.
- 47 M. Oszejka, M. Brindell, Ł. Orzeł, J. M. Dąbrowski, K. Śpiewak, P. Łabuz, M. Pacia, A. Stochel-Gaudyn, W. Macyk, R. van Eldik and G. Stochel, Mechanistic studies on versatile metal-assisted hydrogen peroxide activation processes for biomedical and environmental incentives, *Coord. Chem. Rev.*, 2016, **327–328**, 143–165.
- 48 S. P. Sun and A. T. Lemley, p-Nitrophenol degradation by a heterogeneous Fenton-like reaction on nano-magnetite: process optimization, kinetics, and degradation pathways, *J. Mater. Chem. A*, 2011, **349**, 71–79.
- 49 C. Jasmina Hafizovic, J. Ren, O. Unni, G. Nathalie, L. Carlo, B. Silvia and L. Karl Petter, A new zirconium inorganic building brick forming metal organic frameworks with exceptional stability, *J. Am. Chem. Soc.*, 2008, **130**, 13850–13851.
- 50 Y. Wu, H. Wang, W. Tu, Y. Liu, S. Wu, Y. Z. Tan and J. W. Chew, Construction of hierarchical 2D-2D Zn₃In₂S₆/fluorinated polymeric carbon nitride nanosheets photocatalyst

- for boosting photocatalytic degradation and hydrogen production performance, *Appl. Catal., B*, 2018, **233**, 58–69.
- 51 G. Liu, P. Niu, L. Yin and H. M. Cheng, Alpha-sulfur crystals as a visible-light-active photocatalyst, *J. Am. Chem. Soc.*, 2012, **134**, 9070–9073.
- 52 W. Li, D. Li, Y. Lin, P. Wang, W. Chen, X. Fu and Y. Shao, Evidence for the active species involved in the photodegradation process of methyl orange on TiO₂, *J. Phys. Chem. C*, 2012, **116**, 3552–3560.
- 53 H. Fu, L. Zhang, S. Zhang, Y. Zhu and J. Zhao, Electron spin resonance spin-trapping detection of radical intermediates in N-doped TiO₂-assisted photodegradation of 4-chlorophenol, *J. Phys. Chem. B*, 2006, **110**, 3061–3065.
- 54 X. Hou, X. Huang, Z. Ai, J. Zhao and L. Zhang, Ascorbic acid/Fe@Fe₂O₃: a highly efficient combined Fenton reagent to remove organic contaminants, *J. Hazard. Mater.*, 2016, **310**, 170–178.
- 55 J. Ng, X. Wang and D. D. Sun, One-pot hydrothermal synthesis of a hierarchical nanofungus-like anatase TiO₂ thin film for photocatalytic oxidation of bisphenol A, *Appl. Catal., B*, 2011, **110**, 260–272.
- 56 L. Ai, C. Zhang, L. Li and J. Jiang, Iron terephthalate metal-organic framework: revealing the effective activation of hydrogen peroxide for the degradation of organic dye under visible light irradiation, *Appl. Catal., B*, 2014, **148–149**, 191–200.